energies

MDPI

Article

Variable Valve Strategy Evaluation for Low-Load Operation in a Heavy-Duty Gasoline Compression Ignition Engine

Praveen Kumar * and Yu Zhang

Aramco Americas, Aramco Research Center, Detroit, MI 48377, USA; yu.zhang@aramcoamericas.com
* Correspondence: praveen.kumar@aramcoamericas.com

Abstract: By harnessing gasoline's low reactivity for partially premixed combustion promotion, gasoline compression ignition (GCI) combustion shows the potential to produce markedly improved NOx-soot trade-off with high fuel efficiency compared to conventional diesel combustion. However, at low-load conditions, gasoline's low reactivity poses challenges to attaining robust combustion with low unburned hydrocarbons (UHC) and carbon monoxide (CO) emissions. Increasing the in-cylinder charge temperature by using variable valve actuation (VVA) can be an effective means to address these challenges. In this numerical investigation, VVA strategies, including (1) early exhaust valve opening (EEVO), (2) positive valve overlap (PVO), and (3) exhaust rebreathe (ExReb), were investigated at 1375 RPM and 2 bar brake mean effective pressure in a heavy-duty GCI engine using a market-based gasoline with a research octane number (RON) of 93. The total residual gas level was kept over 50% to achieve an engine-out NOx target of below 1.5 g/kWh. For a complete engine system analysis, one-dimensional (1-D) system-level modeling and three-dimensional (3-D) computational fluid dynamics (CFD) analysis were close-coupled in this study. Performance of the VVA strategies was compared in terms of in-cylinder charge and exhaust gas temperatures increase versus brake-specific fuel consumption (BSFC). The EEVO strategy demonstrated in-cylinder charge and exhaust temperature increase up to 130 and 180 K, respectively. For similar in-cylinder charge temperature gains, the ExReb strategy demonstrated 11% to 18% lower BSFC compared to the EEVO strategy. This benefit primarily originated from a more efficient gas-exchange process. The PVO strategy, due to the valve–piston contact constraint, required excessive exhaust back-pressure valve (BPV) throttling for hot residuals trapping, thereby incurring higher BSFC compared to ExReb. In addition, the ExReb strategy demonstrated the highest potential for exhaust temperature increase (up to 673 K) among the three strategies. This was achieved by ExReb's maximum air-fuel ratio reduction from high internal residuals mass and BPV throttling. Finally, the ExReb profile was optimized in terms of the peak lift, the duration, and the location for maximizing the fuel-efficiency potential of the strategy.

Keywords: variable; valve; residual; exhaust; rebreathing; heavy-duty; low-NOx; GCI; analysis

check for updates

Citation: Kumar, P.; Zhang, Y. Variable Valve Strategy Evaluation for Low-Load Operation in a Heavy-Duty Gasoline Compression Ignition Engine. *Energies* **2022**, *15*, 2017. https://doi.org/10.3390/en15062017

Academic Editor: Adam Smoliński

Received: 8 February 2022
Accepted: 8 March 2022
Published: 10 March 2022

Publisher's Note: MDPI stays neutral with regard to jurisdictional claims in published maps and institutional affiliations.

Copyright: © 2022 by the authors. Licensee MDPI, Basel, Switzerland. This article is an open access article distributed under the terms and conditions of the Creative Commons Attribution (CC BY) license (https://creativecommons.org/licenses/by/4.0/).

1. Introduction

Regulatory pressures and market competition continue to drive commercial applications toward lower-criteria pollutants and lower greenhouse gas emissions [1]. Recent public announcements of future regulatory emission reduction by 50–90% for criteria pollutants, including oxides of nitrogen (NOx), nonmethane hydrocarbons (NMHC), and particulate matter (PM) [2], pose significant challenges to existing combustion and engine aftertreatment (EAT) systems, thereby driving the need for technological evolvement of these systems to meet the future 0.027 g/kWh NOx standard.

To that end, advanced gasoline combustion concepts have been investigated, including a high-efficiency dilute gasoline engine (HEDGE) [3], gasoline direct-injected compression ignition (GDCI) [4,5], and partially premixed compression ignition (PPCI) [6–9]. By implementing low intake temperatures and high charge dilution levels, these combustion strategies leverage gasoline's low reactivity to attain sufficiently premixed combustion, thereby offering a good potential to achieve high fuel efficiency and low engine-out NOx emissions.

Previously, applying the gasoline compression ignition (GCI) concept in a heavy-duty (HD) diesel engine [10–12] appreciably improved NOx-soot trade-off for gasoline fuels with a research octane number (RON) ranging from 60 to 93. At low-load operations, gasoline's low reactivity poses challenges of high combustion efficiency losses and deteriorated combustion stability due to low in-cylinder temperatures. This penalizes the in-cylinder charge mixture's dilution tolerance, thus making engine-out NOx control more challenging. In addition, severe combustion efficiency loss at low-load conditions also reduces exhaust gas temperature, potentially degrading the EAT system performance.

To address these key technical challenges for low-load GCI operations, effective thermal management strategies that can appreciably increase the in-cylinder charge and the exhaust gas temperatures are desirable. Increased cylinder charge temperature promotes combustion stability and lowers unburned hydrocarbons (UHC) and carbon monoxide (CO) emissions via enhanced charge thermal reactivity. Subsequently, a robust combustion process also improves the exhaust gas temperature to enhance the EAT system performance [13–15].

Conventional thermal management strategies, including intake throttling, back-pressure valve (BPV) throttling, retarded main fuel injection timing, intake air heating devices, and thermal insulation, are known to elevate the in-cylinder charge and the exhaust gas temperatures [16]. However, these strategies likely become less favorable in terms of the temperature increase versus brake-specific fuel consumption (BSFC) trade-off under aggressive thermal promotion requirements. Hence, advanced thermal management strategies that can fuel-efficiently elevate the in-cylinder charge and the exhaust temperatures are imperative.

Variable valve actuation (VVA) is known to be an effective means to control the in-cylinder thermal environment. Traditionally, VVA is utilized for improving part-load fuel economy in spark-ignited (SI) engines by reducing intake throttling loss [17,18], and it has been studied for enabling high-efficiency, low-temperature combustion in compression ignition (CI) diesel engines [19–22]. In the past several years, there has been growing interest in utilizing VVA for thermal management, and various investigations have demonstrated its tremendous potential.

Ratzberger et al. [23] investigated variable intake valve (IV) and exhaust valve (EV) strategies for exhaust temperature increase at low-load conditions in a light-duty (LD) diesel engine. The study emphasized the benefits of an early exhaust valve opening (EEVO) strategy on the exhaust gas temperature and the enthalpy increase. During the transient catalyst warm-up, the effectiveness of EEVO for exhaust temperature increase was shown to be equivalent to an electric heater. Similarly, Ding et al. [24] experimented with combinations of EEVO, late intake valve closing (LIVC), and cylinder deactivation (CDA) for exhaust gas temperature increase at the 800 RPM and 0.26 bar brake mean effective pressure (BMEP) condition in a medium-duty diesel engine. EEVO and LIVC showed merit in raising the exhaust gas temperature. When combined with the CDA strategy, the exhaust gas temperature was further increased beyond 523 K, while also reducing fuel consumption by 36% from an efficient gas-exchange process compared to a six-cylinder operation.

Gosala et al. [25] used the EV and the IV phasing for a rapid increase in the exhaust gas temperature during steady-state operations and the transient HD Federal Test Procedure (FTP) cycle. The negative valve overlap strategy when combined with LIVC maximized the level of internal exhaust gas recirculation (int.EGR). Later, Ramesh et al. [26] tested exhaust rebreathing (involving the IV and the EV) to identify a fuel-efficient way to achieve an adequate EAT system temperature near the idle condition in a medium-duty diesel engine. The induction of hot residual gas from the exhaust manifold to the intake manifold resulted in a 2% fuel savings over the HD FTP cycle, via a reduction in pumping mean effective pressure (PMEP) losses. Although, the understanding of VVA strategies for low-load operation is well known for diesel combustion, only limited data has been reported for low-load GCI operations in HD engines. To that end, this study examines the potential of VVA strategies to address key issues of combustion robustness and low exhaust temperature for low-load HD GCI operations, using a RON93 market gasoline.

The current study was carried out with the following objectives:

1. Evaluate performance of a variety of VVAs in terms of the trade-off on in-cylinder and exhaust gas thermal promotion versus fuel efficiency;
2. Develop a tailored VVA strategy for low-load HD GCI operations.

2. Engine Setup

A model-year 2013 Cummins ISX15 heavy-duty diesel engine was modified to build a prototype HD GCI engine, which has been used in previous experimental investigations [10–12]. The same engine served as the base engine in the current study. Figure 1 shows the engine layout. For air and exhaust gas recirculation (EGR) flow management, the engine was equipped with a single-stage variable geometry (VG) turbocharger and a high-pressure EGR (HP EGR) cooler system.

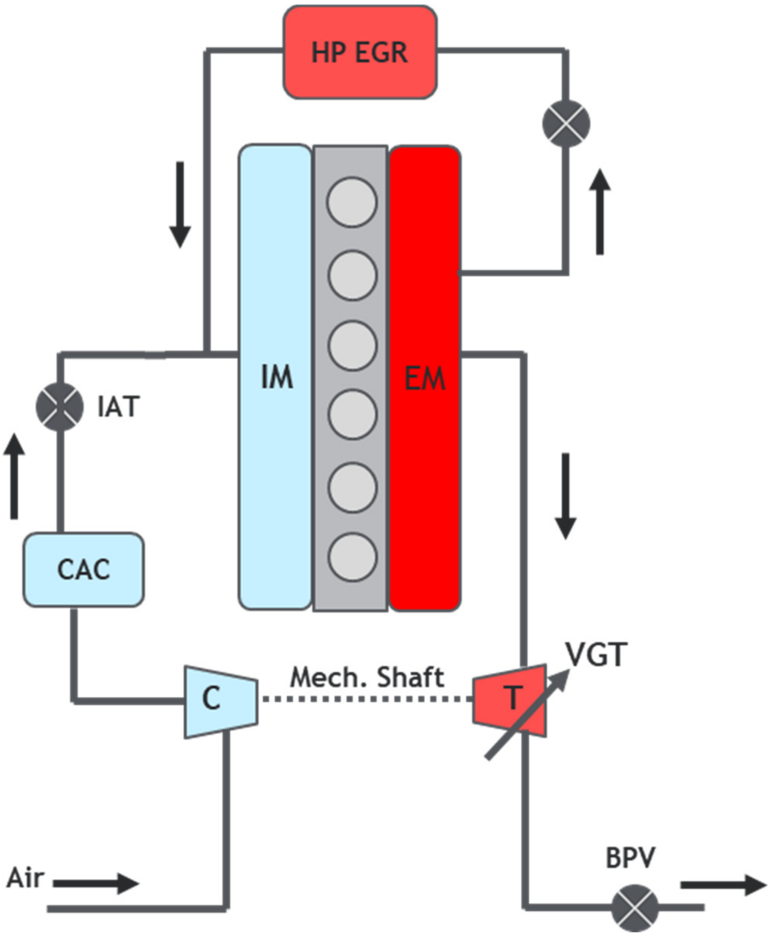

Figure 1. Schematic of the HD GCI engine configuration.

Table 1 shows the engine specifications. In the HD Supplemental Emissions Test (SET) cycle, engine speeds A, B, and C are defined as 1150, 1375, and 1600 RPM, respectively.

Table 1. Engine specifications.

HDGCI Engine Setup Details	
Displacement	14.9 L, 6 Cylinders
Bore	137 mm
Stroke	169 mm
Geometric Compression Ratio	15.7
Air-Handling System	Single-stage variable geometry turbocharger, cooled HP EGR with charge air cooling
Engine Rating	336 kW/1800 RPM

3. Simulation Methodology

The numerical investigation was carried out at the 1375 RPM and 2 bar BMEP (B10) condition, as shown in Figure 2. For this study, a detailed one-dimensional (1-D) engine model representing the HD GCI engine was close-coupled with a three-dimensional (3-D) computational fluid dynamics (CFD) GCI combustion model. Prior to the close-coupling, 1-D and 3-D CFD models were calibrated and verified against GCI test data. The details of the models are discussed in the following sections.

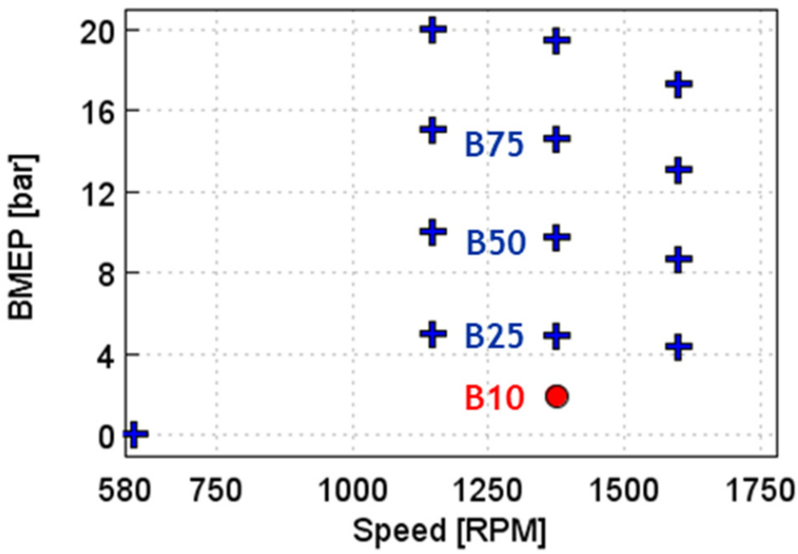

Figure 2. The 13-mode non-idle SET cycle. The investigated B10 condition is highlighted in red.

3.1. 1-D Engine Model

The GT-Power-based [27] 1-D engine model was developed and calibrated for GCI operation using a RON93 gasoline at a geometric compression ratio (CR) of 15.7. The details of the model calibration can be found in Kumar et al. [28,29].

In the 1-D engine model, the capacity of the charge air cooler (CAC) was increased to maintain an intake temperature range of ~338–343 K, a common condition in HD diesel engines. For combustion, the in-cylinder heat-transfer correlation from the "Woschni-GT" model was calibrated, and a value of 0.55 was used for the global heat-transfer multiplier. An exhaust back-pressure valve (BPV) was actuated to impose an exhaust flow restriction equivalent to the stock EAT system.

Figure 3 shows the correlation between the 1-D model predictions and the experimental RON93 gasoline combustion data at the (a) 5 bar BMEP (B25), (b) 10 bar BMEP (B50), and (c) 15 bar BMEP (B75) conditions (refer to Figure 2). The predicted in-cylinder pressure traces showed good agreement with the measurements.

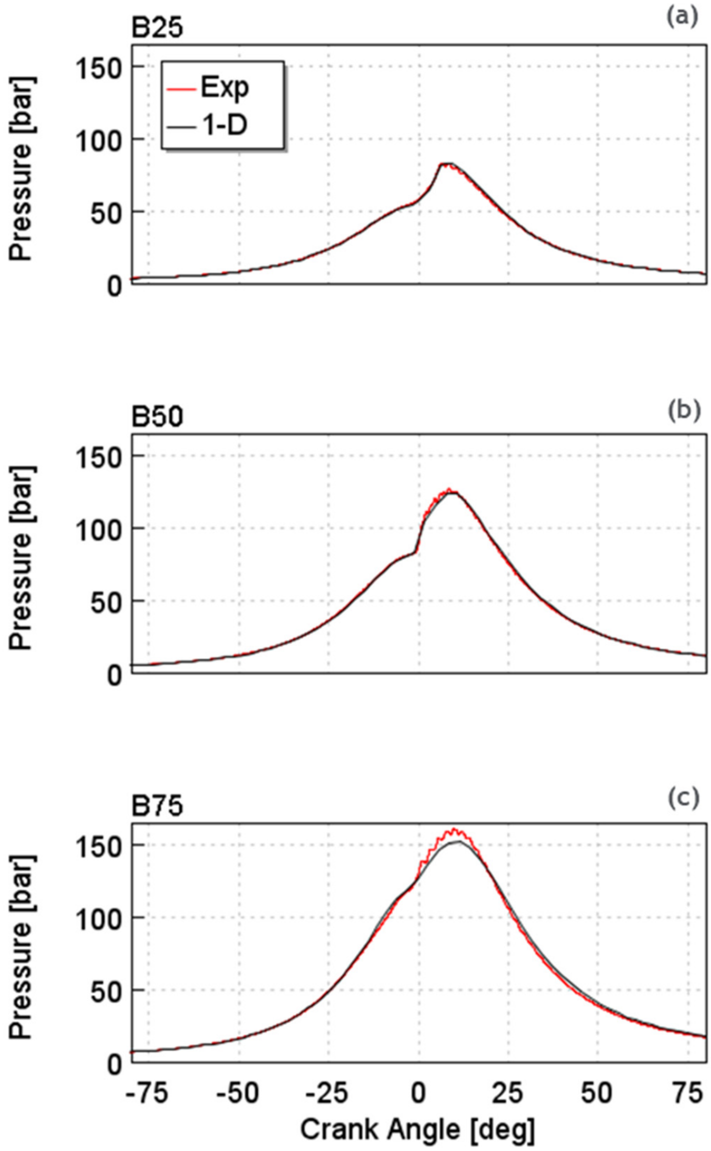

Figure 3. Experiments versus 1-D engine model predictions for closed-cycle in-cylinder pressure at (**a**) B25, (**b**) B50, and (**c**) B75, using RON93 gasoline at CR 15.7.

3.2. 3-D CFD Combustion Model

The low-load GCI combustion strategy was developed by conducting closed-cycle 3-D CFD analysis using the commercially available CFD software CONVERGE [30]. Detailed model setup can be found in the references [12,31].

A primary reference fuel (PRF) blend that was representative of RON93 gasoline was used as the gas-phase surrogate. The reduced PRF mechanism from Liu et al. [32] was used to capture the gas-phase oxidation chemistry, consisting of 44 species and 139 reactions. NOx emissions were simulated using a reduced mechanism of 4 species and 13 reactions, while soot emissions were predicted using a Hiroyaso-NSC two-state soot model. The spray model was calibrated against a gasoline spray characterization data collected using a constant-volume combustion chamber.

The CFD model was validated against the GCI test results for the RON93 gasoline operated at CR 15.7 over a load range of B25→B75 [31]. As seen in Figure 4, the CFD model predictions and the experimental data were in good agreement on both the global combustion behavior and emissions. Building on this CFD model, a combustion strategy development was performed, targeting an engine-out NOx (EO-NOx) below 1.5 g/kWh.

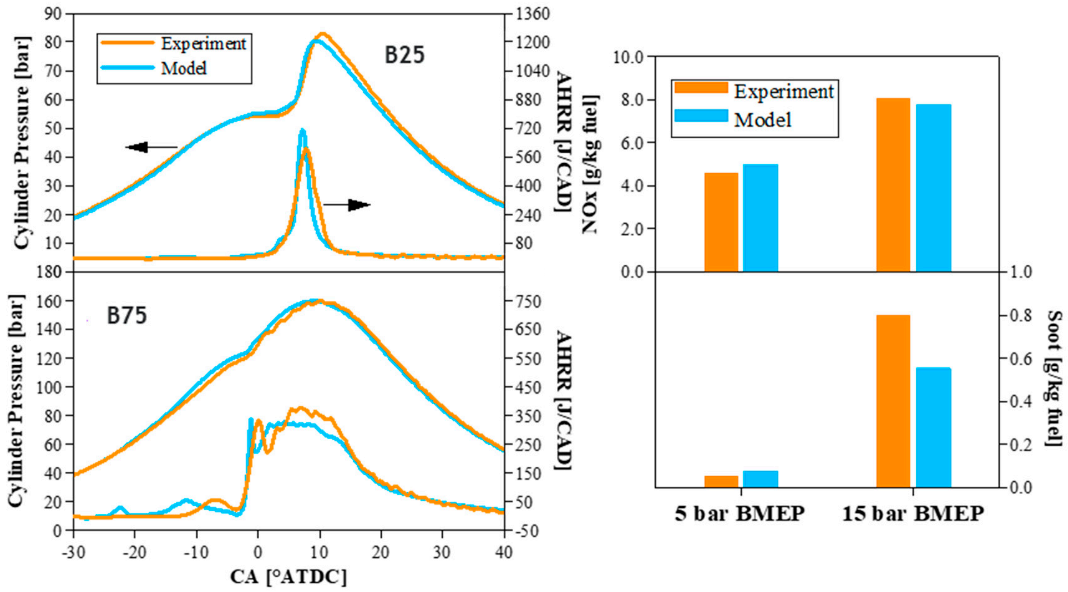

Figure 4. Comparison of cylinder pressure, apparent heat release rate (AHRR), and emissions between the experiments and model results at B25 and B75.

3.3. 1-D and 3-D CFD Models Close-Coupling

As discussed, the 3-D CFD GCI combustion model and the 1-D engine model were close-coupled in this investigation, with the outline shown in Figure 5.

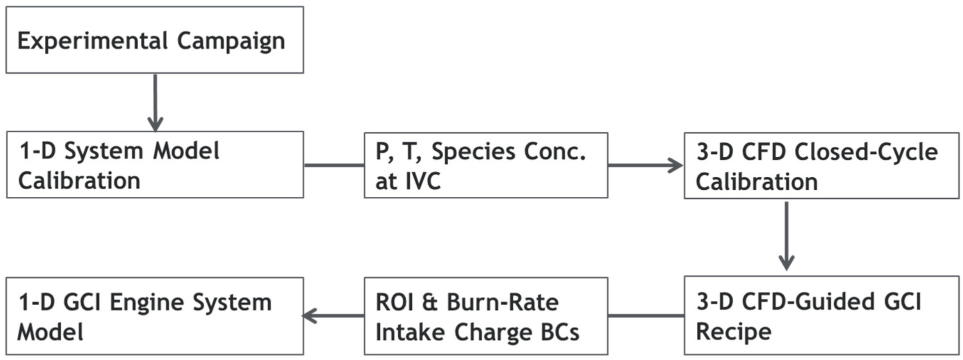

Figure 5. A flowchart of the 1-D and 3-D model close-coupling methodology.

The close-coupling was implemented via the following steps:

The in-cylinder charge conditions at intake valve closing (IVC), obtained from the calibrated 1-D model, were imported into the 3-D CFD model for closed-cycle combustion simulations.

Using the 3-D CFD model, the low-NOx GCI combustion strategy development was performed. Subsequently, the burn-rate (BR) profiles, the fuel rate of injection (ROI) profiles, and the in-cylinder charge-mixture composition at the IVC were extracted and imposed to the 1-D engine model.

An acceptable matching (within 2% error band) of in-cylinder pressure and IVC air-thermal boundary conditions, such as pressure, temperature, O_2, and CO_2 mole fractions, were established between the 1-D and 3-D CFD models, via iterations involving the intake pressure, the intake temperature, and the total residual gas (RSG) mass levels.

Figure 6a,b show the in-cylinder pressure correlations between the 1-D and the 3-D models at B25 and B10, respectively, under high in-cylinder total RSG mass levels. With the peak pressure and charge mixture boundary conditions match within ±2%, a successful close-coupling process was established.

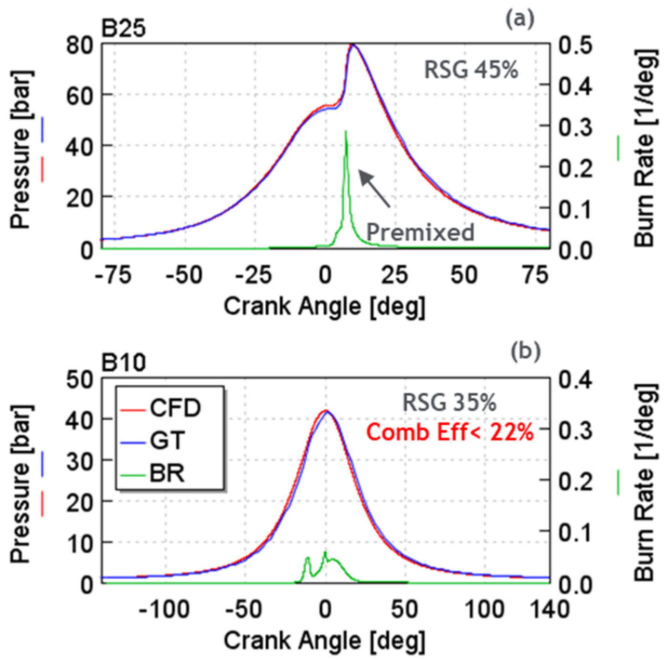

Figure 6. Comparison of in-cylinder pressure between the 1-D and the 3-D models at (**a**) B25 and (**b**) B10 for RON93 gasoline at CR 15.7.

At B25, an intake manifold pressure (IMP) of ~1.2 bar and an in-cylinder temperature before the start of fuel injection (Tsoi) above 835 K led to a robust and a premixed-dominated GCI combustion process, while maintaining the total RSG mass at 45% (Figure 6a). As a result, the predictions showed over 99% combustion efficiency and an EO-NOx below 1.5 g/kWh along with a turbine outlet temperature (TrbOut T) above 573 K, well above the desired minimum exhaust temperature limit of 523 K at the inlet of the oxidation catalyst in the EAT system for HD diesel engines [16].

However, at B10, when simulated with a relatively moderate total RSG mass of ~35% and an in-cylinder charge temperature at the intake valve closing (Tivc) of ~371 K, a severely deteriorated GCI combustion behavior was observed (Figure 6b). Table 2 lists the simulated intake charge conditions and the GCI combustion performance for the B10 condition. Gasoline's autoignition could not be achieved sufficiently under such thermal environment due to its low reactivity. Consequently, the combustion efficiency was reduced to ~22% and the TrbOut T was noted at ~429 K, which was significantly lower than the desired minimum limit of 523 K [16].

Table 2. Simulated GCI performance at B10.

RON93 CR15.7: B10		
Intake Manifold Pressures (IMP)	[bar]	0.96
Intake Manifold Temperature (IMT)	[K]	343
Total Residual Gas (RSG) Mass	[%]	35.14
In-cylinder Charge Temperature at the IVC (Tivc)	[K]	371
In-cylinder Temperature at the Start of Injection (Tsoi)	[K]	773
Combustion Efficiency	[%]	22
Turbine-Out Temperature (TrbOut T)	[K]	429

Therefore, thermal promotion of the in-cylinder charge and the exhaust gases was pursued at the B10 condition by applying VVA strategies. Note that the selection of 371 K as the starting Tivc was intended to adequately investigate the GCI combustion sensitivity to a broad range of the in-cylinder charge temperature and the ensuing implications on implementing VVA strategies. For a quantitative comparison purpose, the B10 performance (shown in Table 2) was termed as "baseline".

4. Variable Valve Actuation Strategy

For the purpose of increasing the Tivc and the TrbOut T, the following VVA strategies were studied:

- Early exhaust valve open (EEVO);
- Positive valve overlap (PVO);
- Exhaust rebreathe (ExReb).

4.1. Early Exhaust Valve Open

The EEVO strategy (Figure 7a), was applied by advancing the baseline EV event. This increased the in-cylinder charge temperature by enabling (1) an early blow-down of high-temperature in-cylinder exhaust gases and (2) a higher in-cylinder total RSG mass via an early exhaust valve closing. On the other hand, the EEVO strategy penalized indicated thermal efficiency (ITEg%) and gas exchange efficiency from the early blow-down of the in-cylinder exhaust gases and recompression of the trapped total RSG mass, respectively. For the present investigation, the EV event was advanced up to 40 crank angle degrees (CAD), as shown in Figure 7a.

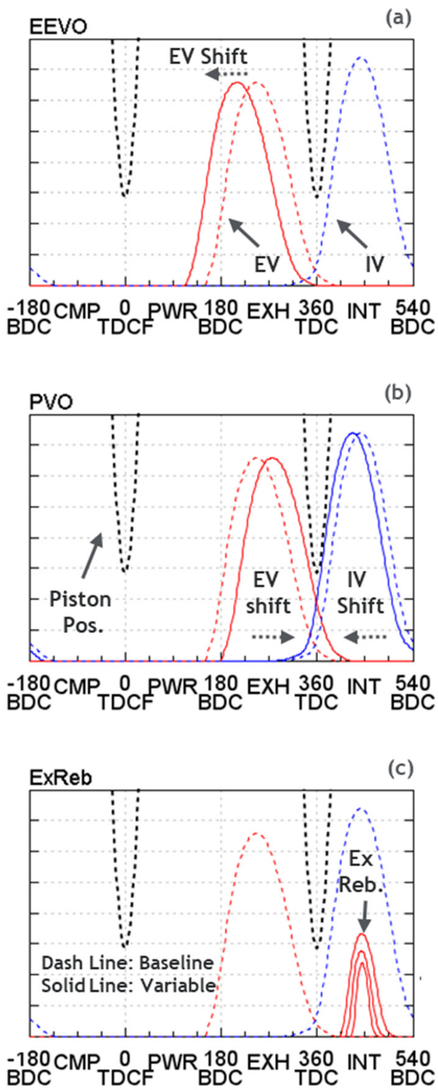

Figure 7. Simulated valve lift profiles for the (**a**) EEVO, (**b**) PVO, and (**c**) ExReb strategies.

4.2. Positive Valve Overlap

The PVO strategy, where the EV and the IV events were retarded and advanced, respectively, was applied to increase the overlap duration between the two events. An increased valve overlap duration increased the in-cylinder total RSG mass by allowing a cross flow of the exhaust gases from the exhaust port to the intake port. For this study, the EV and the IV events were shifted to the maximum allowed positions of the 30 CAD and the 15 CAD, respectively, under the constraint of the valve-piston contact limit, as shown in Figure 7b. In addition, the BPV was throttled to increase the total RSG mass level, when required.

4.3. Exhaust Rebreathe

For the ExReb strategy, a second EV event was implemented during the main IV event, as shown in Figure 7c. In the middle of the intake stroke, the triggering of the second EV event allowed a reverse induction of the exhaust gases inside the cylinder from the exhaust ports, thereby increasing the in-cylinder total RSG mass level. In this study, a wide range of ExReb profiles, with varying durations, locations, and peak lifts, were evaluated.

To maintain a practical viability of the analysis-led VVA strategy design, several mechanical limits (shown in Table 3) were imposed during the investigation.

Table 3. Mechanical Engine System Limits.

HD GCI Engine System Limits		
Compressor Out Temperature	[K]	503
Turbine Inlet Temperature	[K]	1033
Turbine Speed	[kRPM]	200
Peak Cylinder Pressure	[bar]	200
Exhaust Manifold Pressure	[bar]	5
Maximum Pressure Rise Rate	[bar/CAD]	12

5. Results and Discussion

The complete engine system analysis was conducted in the following three parts:
Part 1: Closed-Cycle 3-D CFD Analysis;
Part 2: 1-D System Level VVA Analysis;
Part 3: Strategy Optimization.
Each part is discussed in the subsequent sections.

5.1. Part 1: Close-Cycle 3-D CFD Analysis

In part 1, starting off at the baseline condition of a Tivc of 371 K (show in Table 2), a 3-D CFD-led low-NOx GCI closed-cycle combustion analysis was conducted at elevated Tivc levels up to 446 K. This range of Tivc was investigated not only to identify a feasible air thermal boundary condition to attain a robust combustion operation but also to understand the full extent of the effects of Tivc promotion on the closed-cycle combustion and the engine system performance.

For this campaign, a tailored GCI combustion system design was used [12]. At B10, using an injection pressure of 300 bar, a double injection strategy was applied where the total fuel quantity was split by 65:35 ratio between first (pilot) and second (main) injection events. The pilot injection was timed at the 25 CAD before top-dead-center firing (TDCF) followed by the main injection event at the 8 CAD before the TDCF.

Table 4 shows the range of Tivc and other key performance parameters for the closed-cycle GCI combustion analysis targeting the EO-NOx below 1.5 g/kWh. As expected, increase in the Tivc level improved the GCI combustion performance. The results showed, increasing Tivc beyond 400 K dramatically improved the combustion efficiency and the GCI combustion robustness by enabling an advanced combustion phasing (CA50).

Table 4. Closed-cycle B10 performance at elevated Tivc levels.

RON93 CR15.7: B10				
		Case 1	Case 2	Case 3
Closed-Cycle Results				
Tivc	[K]	404	412	446
Start of Injection: Pilot and Main	[° aTDC]	−25 and −8		−30 and −8
Fuel Injection Pressure	[bar]	300		
Total Fuel Split: Pilot and Main	[-]	65:35		
Total Residual Gas (RSG) Mass	[%]	52.5	52.6	52.0
Combustion Phasing (CA50)	[CAD]	10.8	6.5	0.6
Combustion Efficiency	[%]	>99	>99	>99
Indicated Thermal Efficiency (ITEg)	[%]	49.9	50.3	48.9

For Tivc 404 K, the combustion efficiency was increased beyond 99% and the CA50 was advanced to the ~11 CAD after the TDCF, while maintaining the total RSG mass over 52%. When the Tivc was increased to 412 K, the CA50 further advanced to the 6.5 CAD after the TDCF, resulting in a shorter combustion duration and an increased ITEg%. The peak ITEg% of 50.3% was predicted for the Tivc level of 412 K.

Interestingly, Tivc of 446 K showed a markedly shortened combustion duration and the CA50 in a closed proximity to the TDCF. This caused excessive cylinder temperature during combustion, leading to increased in-cylinder heat transfer losses and thereby resulting in an ITEg% loss of 1.4% (from Table 4) compared to the Tivc 412 K case. Figure 8a–c shows the burn rate (BR), normalized rate of fuel injections (ROI), and the in-cylinder pressure for the Tivc 404, 412, and 446 K levels, respectively. From Figure 8, effects of Tivc increase on the combustion duration, CA50, and the peak cylinder pressure corroborate the increasingly efficient GCI combustion process at elevated Tivc levels.

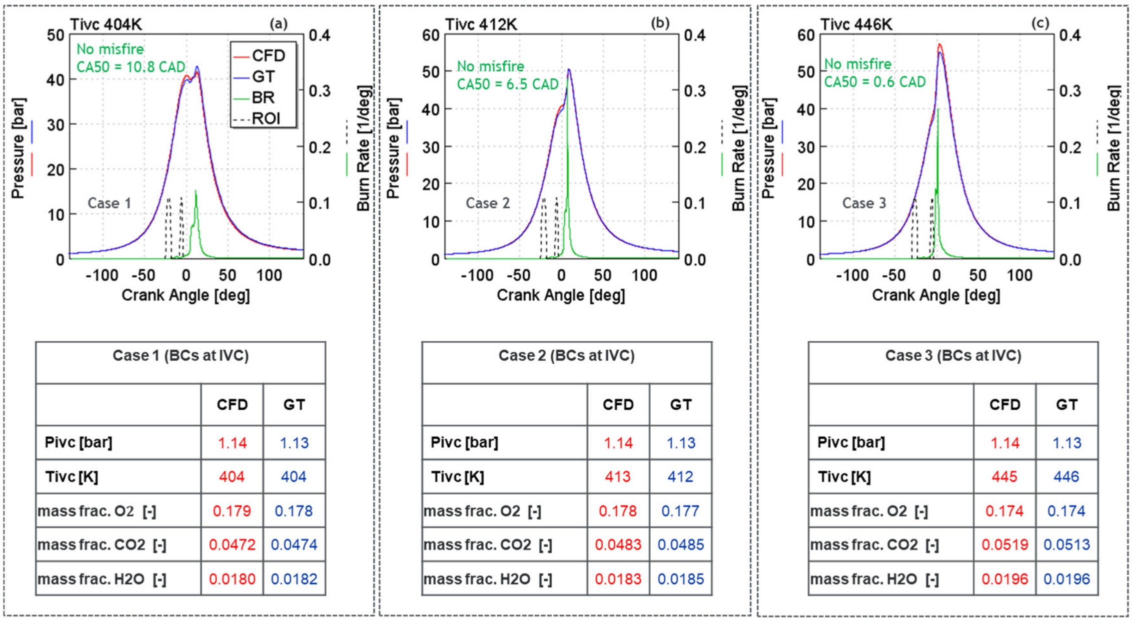

Figure 8. In-cylinder pressure traces and air-thermal boundary conditions comparison between 1-D and 3-D CFD models for (**a**) Tivc 404 K, (**b**) Tivc 412 K and (**c**) Tivc 446 K.

Moreover, for each Tivc case, the 1-D engine model predictions were compared with the 3-D CFD results. The 1-D model predicted in-cylinder pressure traces were noted within ±2% of the 3-D CFD results for Tivc 404 K, 412 K and 446 K as shown in Figure 8a–c, respectively. In addition, the air-thermal boundary conditions, including the in-cylinder pressure at the IVC (Pivc), Tivc, and the in-cylinder charge composition (CO_2, O_2, and H_2O mass fractions) at the IVC, also correlated well between the 1-D and the 3-D CFD models (Figure 8).

The established correlation for the Tivc range of 404 to 446 K (Figure 8) confirmed a high-fidelity close-coupling of the 1-D and the 3-D CFD models, thus proving a reliable foundation for the 1-D engine model to carry out a detailed system-level VVA analysis, as discussed in the next section.

5.2. Part 2: 1-D System-Level VVA Analysis

In part 2, using the 1-D engine model, VVA strategies, including EEVO, PVO, and ExReb (shown in Figure 7), were evaluated to achieve the Tivc targets of 404, 412, and 446 K. While delivering the Tivc targets, the corresponding total RSG mass was maintained to the level shown in Table 4. The three strategies were compared in terms of int.EGR requirement, EV and IV flow trends, in-cylinder temperature trend, air–fuel ratio (AFR) reduction, gas-exchange efficiency, and exhaust temperature increase as discussed in the following sections.

5.2.1. Internal EGR Comparison

All the three VVA strategies resulted in Tivc increase via adequate trapping of the int.EGR portion. Table 5 shows the valve event variability and the BPV positions for the EEVO, PVO, and ExReb strategies that delivered the Tivc levels of 404, 412, and 446 K.

Table 5. Implemented valve variability and the BPV positions for the EEVO, PVO, and ExReb strategies at B10.

	Simulated Tivc Levels [K]								
	404			412			446		
	EEVO	PVO	ExReb1	EEVO	PVO	ExReb2	EEVO	PVO	ExReb3
EV/IV Shift [° aTDC]	−12/0	30/−15	-	−14/0	30/−15	-	−18/0	30/−15	-
BPV [% Open]	77	67	77	91	62	91	100	49	100
ExReb-to-Main Lift Ratio [−]	-	-	0.36	-	-	0.42	-	-	0.50

For EEVO, with the increasing trapped int.EGR via advancing of the EV event, the BPV became increasingly relaxed to reduce the external EGR (ext.EGR) portion and maintain the total RSG mass unchanged. The turbine rack remained fully open. From Table 5, the PVO strategy was exercised by retarding the EV and advancing the IV by the 30 CAD and the 15 CAD, respectively. When implementing PVO, the BPV was increasingly throttled (from 67% to 49% position), while the HP EGR valve was proportionally closed to increase the int.EGR portion and maintain the desired total RSG mass for each Tivc level.

For ExReb, three different rebreathe strategies—ExReb1, ExReb2, and ExReb3—were applied (refer to Table 4), where the percent of the rebreathing profile lift to the main exhaust valve lift was implemented at 36%, 42%, and 50%, respectively. These ratios were determined by a design-of-experiments (DoE) campaign to achieve the Tivc 404, 412, and 446 K levels, while maintaining the BPV throttling identical to those for EEVO.

Figure 9 compares the resulting trapped int.EGR portions among the three VVA strategies that produced Tivc of 404, 412, and 446 K. For the baseline case, the int.EGR level is also shown for reference. As expected, increasing the int.EGR portion helped increase the Tivc from the baseline Tivc of 371 K that contained int.EGR portion below ~5%.

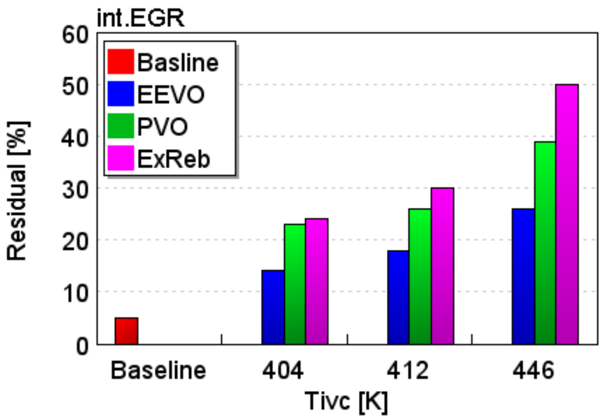

Figure 9. Comparison of int.EGR portions requirements among the strategies at different Tivc levels.

Interestingly, among the three strategies, the EEVO strategy showed the lowest int.EGR portion requirement to achieve a given Tivc level, whereas the ExReb strategy required the highest int.EGR portion. For example, at Tivc 404 K, the int.EGR portion difference between the two strategies was noted at 10%; however, at Tivc 446 K, the difference increased to more than 25%. Furthermore, the PVO strategy demonstrated a relatively modest int.EGR range of 23–39%, compared to the ExReb strategy. For a given Tivc level, the difference in the int.EGR portion requirement for the EEVO, PVO, and ExReb strategies implied differences in the underlying mechanism of thermal promotion. To understand the mechanism and explain the differences in the int.EGR portion requirement, the EV and IV flow trends were next evaluated.

5.2.2. Valve Flow Trends Comparison

The EV and IV flow trends for the EEVO, PVO, and ExReb strategies are plotted in Figure 10a–c, respectively, for the Tivc 404 K case.

For the EEVO strategy, shown in Figure 10a, advancing of the EV by 12 CAD allowed an early blow-down of the in-cylinder hot exhaust gases and trapping of the hot residual gases due to early exhaust valve closing. The increased trapped hot residual mass, via advancing EEVO, experienced recompression near the TDC gas-exchange (360 CAD), resulting in a large reverse flow through the intake valve, as observed in Figure 10a. This caused the intake port temperature to increase to 378 K (over 30 K higher than the baseline 345 K level) and consequently elevated the Tivc to 404 K. Due to high exhaust gas temperatures from the early blow-down event, only a 14% int.EGR portion was needed, as observed in Figure 9.

In the PVO strategy (Figure 10b), the maximized EV and IV overlap area near the TDC gas-exchange (360 CAD) and the BPV position of 67% (shown in Table 5) facilitated a cross flow of exhaust gases from the exhaust port to the intake port, as suggested from the reverse flow through the EV and IV. Due to relatively cooler exhaust gas temperature from higher expansion work for the PVO strategy, the cross flow led to an intake port temperature of 365 K, ~13 K cooler than the EEVO counterpart. Therefore, an int.EGR portion of 23% was required for the PVO strategy (shown in Figure 9).

For the ExReb strategy (Figure 10c), a second EV event was applied during the IV duration. This allowed a reverse induction of the exhaust gases from the exhaust port to the cylinder. For this strategy, negligible reverse flow of the exhaust gases through the intake valve was noted, therefore negligible effect was expected on the intake port temperature. However, due to continued intake stroke, the in-cylinder charge temperature was expected to further cool down, thereby requiring an int.EGR portion of 24%, the highest level among the three strategies (noted in Figure 9).

With the similar mechanism, the differences of the valve flow trends among the strategies increased at elevated Tivc levels, leading to increasingly different int.EGR portions at Tivc 412 and 446 K (observed in Figure 9).

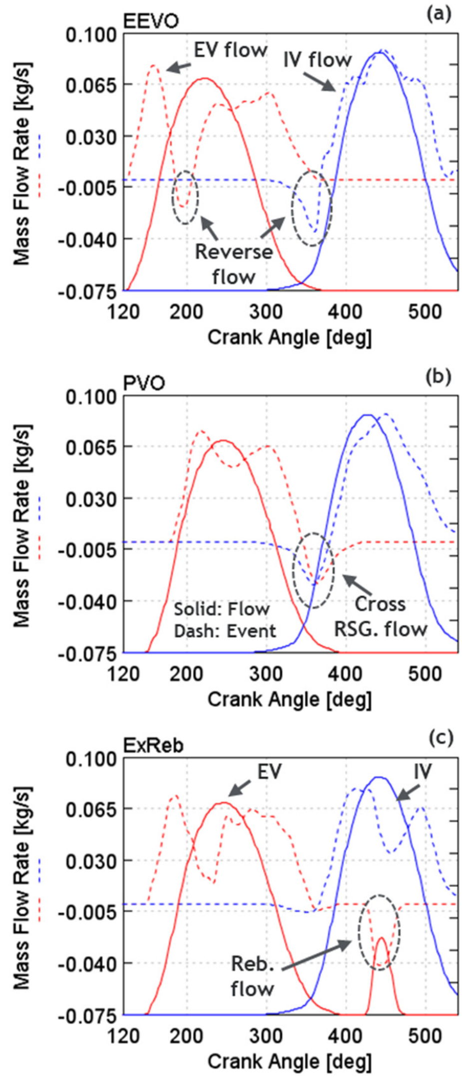

Figure 10. EV and IV flow trends for the (**a**) EEVO, (**b**) PVO, and (**c**) ExReb strategies for Tivc of 404 K at B10.

5.2.3. In-Cylinder Temperature Comparison

To corroborate the observed EV and IV flow trends with the in-cylinder charge thermal promotion, the in-cylinder temperature traces were compared among the EEVO, PVO, and ExReb strategies at the lowest Tivc target of 404 K and the highest Tivc target of 446 K, as shown in Figure 11a,b, respectively. The in-cylinder temperature trend for the baseline case was also plotted for reference.

Figure 11a, advancing of the EV event for the EEVO strategy (refer to Table 5), shows a rapid decline of the in-cylinder temperature down to 583 K at the 180 CAD. This was due to the early blow-down of the in-cylinder exhaust gases, as discussed in the previous section. However, prior to the intake stroke (near ~350 CAD), the in-cylinder temperature elevated up to 700 K due to the increased trapping of hot int.EGR and its recompression from early exhaust valve closing, which resulted in the Tivc level of 404 K.

Moreover, for the PVO strategy, the facilitated cross flow of the hot exhaust gas (discussed in the previous section) led to an in-cylinder temperature increase up to 600 K near the TDC gas-exchange that primarily elevated the Tivc to the 404 K level, as evident in Figure 11a. As expected for the ExReb strategy, the reverse induction of the exhaust gases from the rebreathe event increased the in-cylinder temperature to ~418 K at the peak IV lift location during the intake stroke that finally led to Tivc of 404 K (Figure 11a). As anticipated for the baseline case, in the absence of a thermal promotion strategy, the in-cylinder temperature at the TDC gas-exchange was noted near 420 K, thereby leading to the baseline Tivc of 371 K (refer to Table 2).

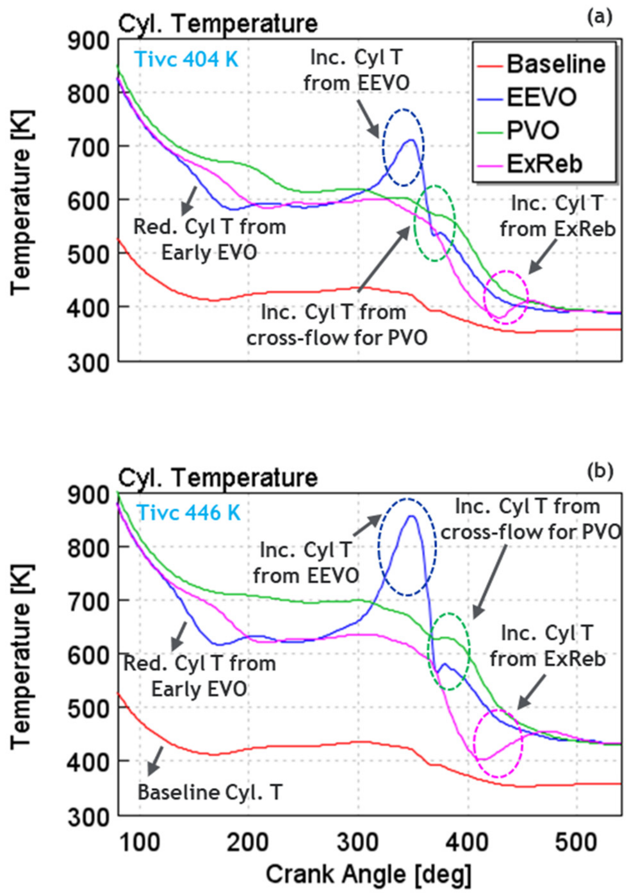

Figure 11. In-cylinder temperatures comparison among the three strategies for Tivc (**a**) 404 and (**b**) 446 K at B10.

The in-cylinder temperature trends among the VVA strategies were compared at the Tivc 446 K level (Figure 11b). Following the individual mechanism, the variation in the in-cylinder temperatures traces among the three strategies were magnified due to enlarged difference in the int.EGR portions (as noted in Figure 9).

As evident in Figure 11b, the EV shift of 18 CAD for the EEVO strategy (see Table 5), led to an in-cylinder temperature increase to 850 K prior to the intake stroke start (near ~350 CAD) that resulted in the Tivc 446 K level. Furthermore, for the PVO strategy, the facilitated cross flow of the hot exhaust gas led to an in-cylinder temperature of over 640 K near the TDC gas-exchange that primarily increased the Tivc to the 446 K level. Similarly, for the ExReb strategy in Figure 11b, the reverse induction of the exhaust gases from the rebreathe event increased the in-cylinder temperature to ~455 K, equivalent to the EEVO and PVO strategies, during the intake stroke and led to the Tivc 446 K level.

5.2.4. AFR and Tsoi Trends Comparison

The increase in the trapped int.EGR portions and the BPV throttling were expected to affect the in-cylinder trapped fresh air flow thus affecting the AFR and the Tsoi due to impacted richness of the in-cylinder charge mixture.

Figure 12a,b compare the AFR and the Tsoi trends, respectively, among the three strategies. The baseline case was also plotted for reference. As expected, due to the increased trapped int.EGR portions, all the three strategies consistently demonstrated reduced AFR from the baseline AFR level of 38.8. The EEVO strategy showed a moderate AFR reduction range of 35.4–33.1 for the Tivc 404–446 K levels. This moderate AFR impact was mainly due to the modest int.EGR portions utilized (observed in Figure 9) and the most relaxed BPV positions (shown in Table 5).

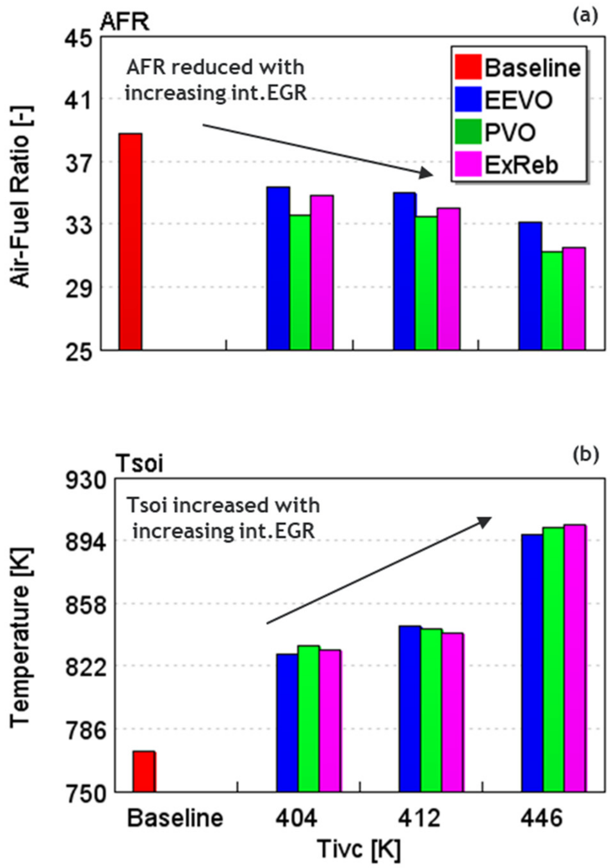

Figure 12. Comparison of (**a**) AFR and (**b**) Tsoi among the EEVO, PVO, and ExReb strategies at different Tivc levels.

On the other hand, for the Tivc 404–446 K levels, the PVO strategy incurred AFR reduction down to 31.2. This was due to the combined impact of the high int.EGR portions (shown in Figure 9) and excessive BPV throttling (shown in Table 5), thereby leading to the lowest in-cylinder trapped air mass and the total engine flow. Interestingly, the ExReb strategy, with the BPV positions identical to the EEVO counterparts, suffered a significant reduction in the AFR levels at a given Tivc. This observed AFR reduction for the ExReb strategy was primarily due to the high int.EGR portions (as noted from the reduced intake valve flow shown in Figure 10c) compared to EEVO.

Tsoi trends were observed to be directly related to the AFR trends (Figure 12b). The AFR reduction caused an increasingly richer combustion, thereby increasing the peak cylinder temperature that raised the in-cylinder exhaust gas temperature (as shown in Figure 11) and led to an increase in Tsoi. Consistent with the AFR trends, the highest Tsoi gain of ~130 K was observed for the Tivc 446 K level. Among the three strategies, the Tsoi trends noted were similar due to nearly identical Tivc, as anticipated.

5.2.5. Gas-Exchange Comparison

The observed differences in the valve flow trends and the underlying mechanism for int.EGR trapping (shown in Figure 10) were bound to cause a difference in the gas-exchange efficiency, thereby affecting the PMEP among the EEVO, PVO, and ExReb strategies. Figure 13 compares the PMEP trends among the strategies at different Tivc levels. Interestingly, at a given Tivc level, the EEVO strategy consistently incurred the highest pumping losses, whereas the ExReb strategy demonstrated the lowest PMEP. The EEVO strategy demonstrated 43% and 72% higher PMEP levels at Tivc 404 and 446 K, respectively, over the ExReb strategy. The large PMEP for the EEVO strategy was attributed to the increased cylinder pressure caused by the recompression of the trapped exhaust gases.

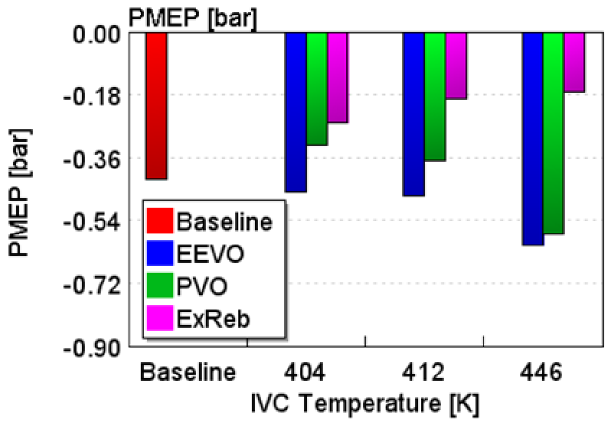

Figure 13. PMEP comparison among the EEVO, PVO, and ExReb strategies at different Tivc levels.

On the other hand, the PVO strategy demonstrated moderately higher PMEP levels with the increasing Tivc, relative to the ExReb strategy. This was primarily attributed to the increasingly aggressive BPV throttling implemented for the PVO strategy (as shown in Table 5).

To corroborate the observed PMEP trends, LogP-LogV trends for the EEVO, PVO, and ExReb strategies were compared for the Tivc 404 and 446 K levels, respectively (Figure 14a,b).

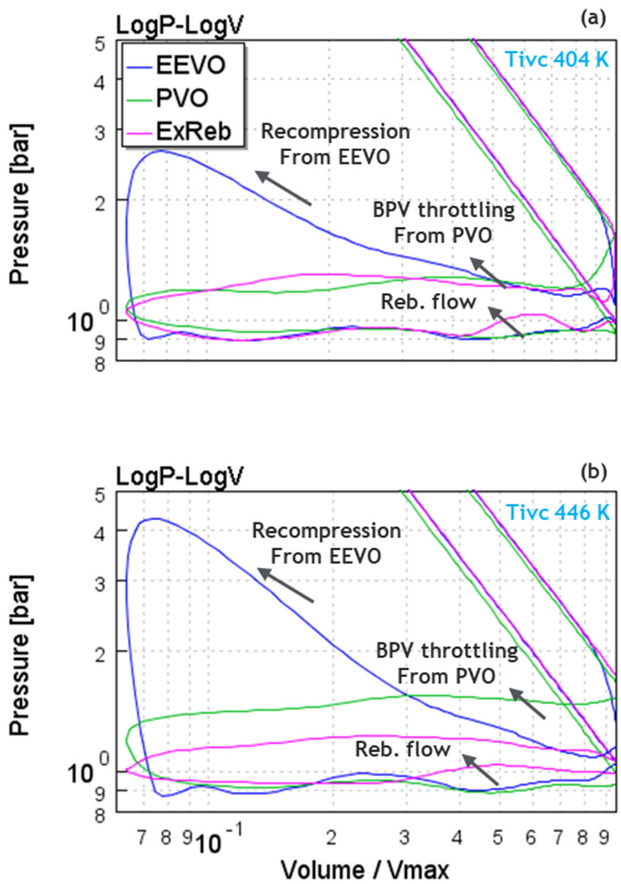

Figure 14. LogP-LogV trends at (**a**) Tivc 404 and (**b**) Tivc 446 K cases for the EEVO, PVO, and ExReb strategies.

Evidently, unlike other strategies, due to recompression of the trapped in-cylinder total RSG mass (see Figure 11), the EEVO strategy led to a significantly large cylinder pressure buildup during the exhaust stroke, thereby incurring the highest PMEP levels for both Tivc cases (shown in Figure 14a,b). Compared to EEVO, the ExReb strategy, managed a significantly lower cylinder pressure during the exhaust stroke due to a relatively lower total engine flow caused by high int.EGR portion levels (see Figure 9). In addition, the reverse induction of the exhaust gas helped elevate the intake cylinder pressure (shown in Figure 14a,b) and further reduced the gas-exchange loop for ExReb, thereby resulting in the lowest PMEP levels. Moreover, for the PVO strategy, excessive BPV throttling, applied to increase the int.EGR portion, caused higher cylinder pressure buildup during the exhaust stroke and reduced the in-cylinder flow (discussed in Figure 10) that led to a larger PMEP level, compared to the ExReb strategy.

Overall, among the three strategies, the ExReb strategy appears to be the best candidate in terms of the desired thermal and flow boundary conditions (Table 5) delivery and PMEP levels. Next, a detailed investigation was performed for further optimization of the rebreathe valve event, as discussed in the following section.

5.3. Strategy Optimization

In this investigation, the exhaust rebreathe strategy was characterized for the following:

- Performance comparison for different rebreathe profiles;
- Effects of rebreathe profile location;
- Lift versus duration trade-off.

Each investigation is discussed in the subsequent sections.

5.3.1. Performance Comparison for Different Rebreathe Profiles

Three different exhaust rebreathe strategies—ExReb1, the ExReb2, and the ExReb3 (refer to Figure 7c)—were simulated for the int.EGR portion sweep up to 50% and compared in terms of the PMEP penalty. The BPV throttling was adjusted as needed to increase the int.EGR portions for each ExReb event. Figure 15 compares the int.EGR portion versus PMEP trends among the three ExReb strategies. For ExReb1, the int.EGR portion increased from 22% to 50% at the expense of increased PMEP from 26 to 65 kPa. On the other hand, with a larger valve lift and duration, the ExReb2 strategy demonstrated ~50% lesser PMEP due to more relaxed BPV throttling, compared to ExReb1. However, in spite of keeping the BPV and the HP EGR valve nearly fully open, the ExReb2 profile struggled to reduce the int.EGR portion below 25%, resulting in a likely overpromotion of Tsoi ~12 K. For ExReb3, while the int.EGR portion of 50% was delivered most efficiently, an int.EGR portion below 30% could not be achieved, causing ~40 K hotter Tsoi compared to the ExReb1 strategy.

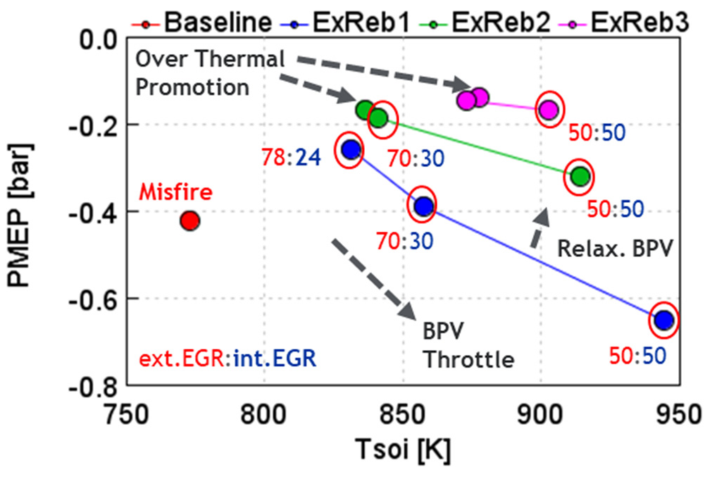

Figure 15. PMEP versus Tsoi trends among the ExReb1, ExReb2, and ExReb3 strategies.

The challenge of int.EGR portion control associated with the larger rebreathe events would likely lead to thermal overpromotion of the in-cylinder charge mixture that potentially risks breaching the maximum pressure rise rate (MPRR) limit (refer to Table 3) and incurring higher heat transfer losses (refer to Table 4) during combustion. Furthermore, the challenge of internal residual gas control for the ExReb2 and ExReb3 strategies would likely result in a higher cylinder-to-cylinder residual gas imbalance (shown in Appendix A Figure A1).

Therefore, ExReb1 (36% of the main peak lift) was determined to be the most appropriate rebreathe lift profile compared to ExReb2 and ExReb3.

5.3.2. Rebreathe Profile Location Optimization

Fundamentally, to facilitate exhaust rebreathing, a large pressure difference between the exhaust port and the cylinder pressure is desirable. Therefore, the inducted residual mass and the PMEP levels are expected to be sensitive to the rebreathe profile location. For an optimized rebreathe profile location, simulations were conducted where the ExReb1 profile was advanced and retarded by the 50 CAD from its current location of the center of the intake valve duration. For an accurate profile location impact, the turbine rack and the BPV positions were fixed (refer to Table 5).

Figure 16a–c compares the exhaust port and cylinder pressure traces for the ExReb1 locations at the advanced 50 CAD, the center of the intake valve, and the retarded 50 CAD, respectively. The piston velocity traces were also plotted for reference. For the center location (Figure 16b), the rebreathe event appeared synchronized with the piston velocity where the peak lift of the rebreathe valve occurred near the maximum piston velocity. The maximum piston velocity led to an appreciable pressure difference between the cylinder and exhaust port by reducing the cylinder pressure, as observed in Figure 16b. In contrast, for the advanced 50 CAD (Figure 16a) and the retarded 50 CAD (Figure 16c) locations, the piston velocity appeared to be reduced by ~50% from its peak level, thereby generating a relatively smaller pressure difference between the cylinder and the exhaust port.

As a result, a nearly 1.5–2% lower int.EGR portion was trapped when the rebreathe valve was located at the advanced 50 CAD and the retarded 50 CAD locations (Figure 17). Consequently, the Tsoi for the advanced 50 CAD and the retarded 50 CAD locations were ~10–12 K lower compared to the center location. Furthermore, the center location resulted in the lowest PMEP due to a larger reduction in the total engine flow from the increased int.EGR trapping. Overall, the center rebreathe profile location demonstrated the best performance.

5.3.3. Lift versus Duration Trade-Off

It is expected that effective valve area for the rebreathe profile, dictated by its peak lift and duration, is instrumental in defining its effectiveness for int.EGR trapping. To determine an optimized rebreathe profile shape, the performance trade-off between the peak lift and the duration must be understood.

Therefore, performance of two exhaust rebreathe profiles, ExReb1 and ExReb1b, with difference in the peak lift and the duration while maintaining an identical effective valve area, were evaluated in terms of int.EGR trapping versus PMEP. The ExReb1b profile consisted of a 66% higher peak lift and a 20 CAD shorter duration compared to the ExReb1 profile. Figure 18a,b compares the cylinder and exhaust pressure traces and the valve flow trends, respectively, between the two rebreathe profiles.

The ExReb1b profile inducted nearly 2% lesser residual mass (Figure 18b) and experienced higher fluctuation in the exhaust pressure (Figure 18a) compared to ExReb1. Consequently, as shown in Figure 19, the ExReb1b profile showed ~15 K reduction in the Tsoi due to lower rebreathe flow, and a ~2.5 kPa higher PMEP level originated from the increased cycle-averaged exhaust pressure.

Evidently, the larger duration and short peak lift rebreathe profile (ExReb1) demonstrated the best trade-off between rebreathe flow and PMEP compared to the short duration and high peak lift profile.

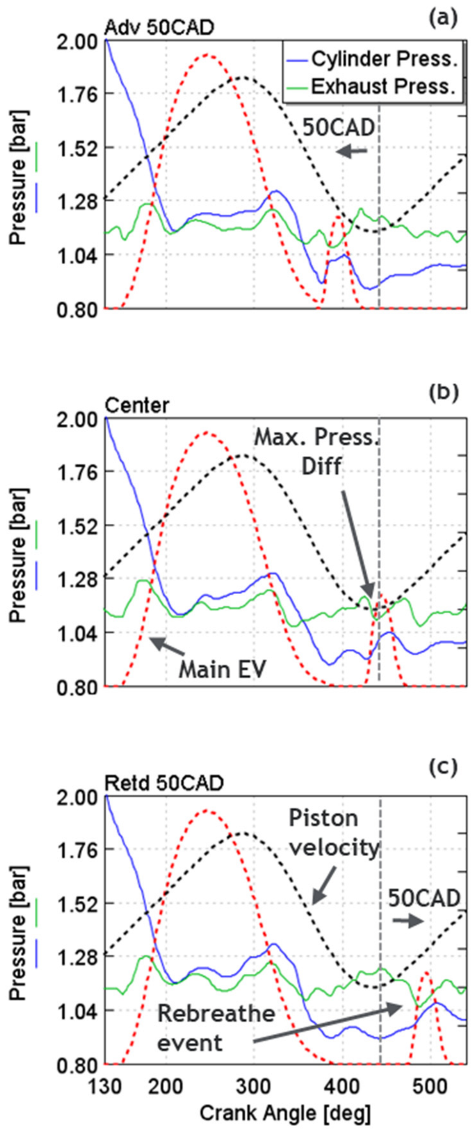

Figure 16. The cylinder and the exhaust pressure traces for the ExReb locations of (**a**) advanced 50 CAD, (**b**) center, and (**c**) retarded 50 CAD for Tivc 404 K at B10.

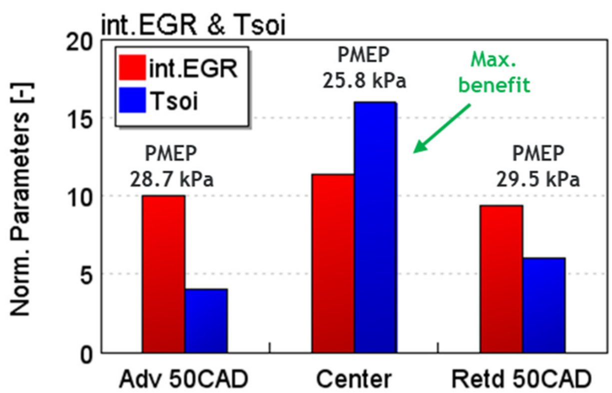

Figure 17. Comparison of Int.EGR and Tsoi trends among the three rebreathe locations for Tivc 404 K at B10. PMEPs are also identified for each location.

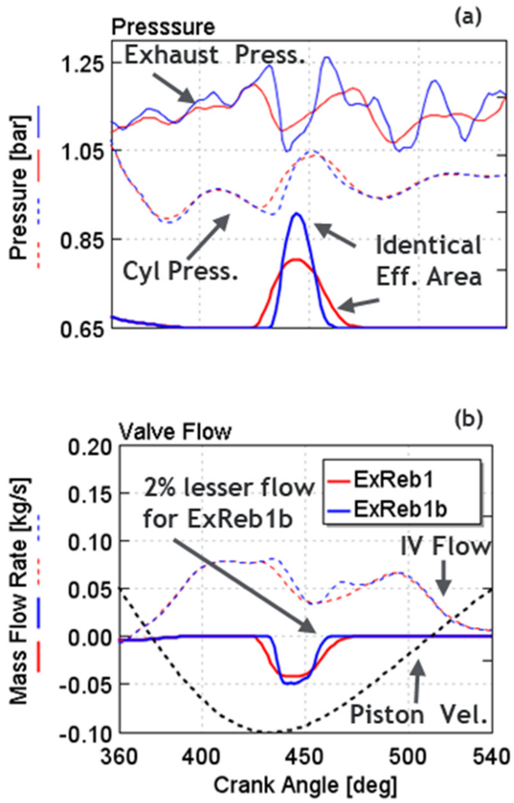

Figure 18. Comparison of (**a**) cylinder and exhaust pressure trends and (**b**) valve flows trends between the ExReb1 and the ExReb1b profiles for Tivc 404 K at B10.

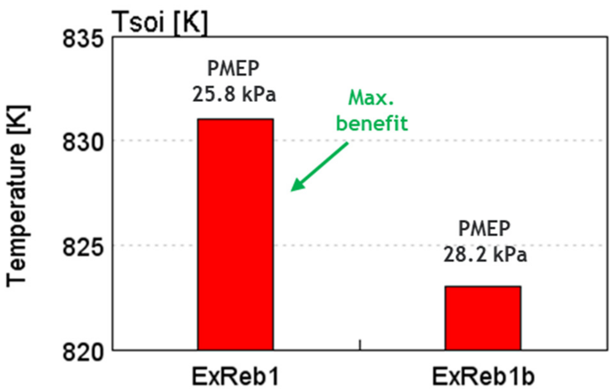

Figure 19. Comparison of the Tsoi and the PMEP trends between the ExReb1 and ExReb1b profiles.

5.4. HP EGR Cooler Bypass

A HP EGR cooler bypass (EGRByp) strategy was also investigated for the intake charge temperature increase. Previous studies [33,34] have reported favorable thermal promotion performance by utilizing uncooled ext.EGR flow. To implement this strategy, the hot exhaust gas from the exhaust manifold (upstream of the HP EGR cooler shown in Figure 1) was bypassed from the EGR cooler and introduced into the mixer and the intake manifold. This led to an intake port temperature increase of ~30 K. Figure 20 compares the trends for total RSG mass level and the Tivc between the baseline case (no bypass) and the EGRByp strategy. As evident from Figure 20, due to increase in the intake port temperature, the EGRByp strategy successfully achieved the Tivc 404 K level, similar to the levels achieved by the three VVA strategies. Consequently, for the Tivc 404 K case, the AFR and Tsoi trends for the EGRByp strategy were comparable to the VVA strategies (shown in Figure 12).

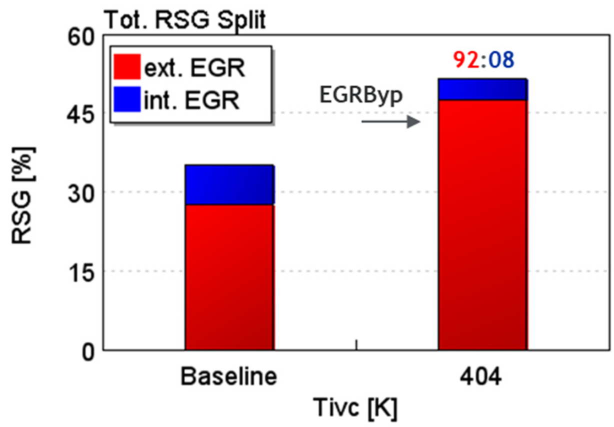

Figure 20. Total residual split between ext.EGR and int.EGR and Tivc, corresponding to the EGRByp strategy at B10.

From Figure 21, due to the unthrottled BPV position, the observed PMEP level was lower than for the ExReb strategy. Nevertheless, the EGRByp strategy failed to achieve Tivc levels beyond 404 K, thus highlighting its practical limitations.

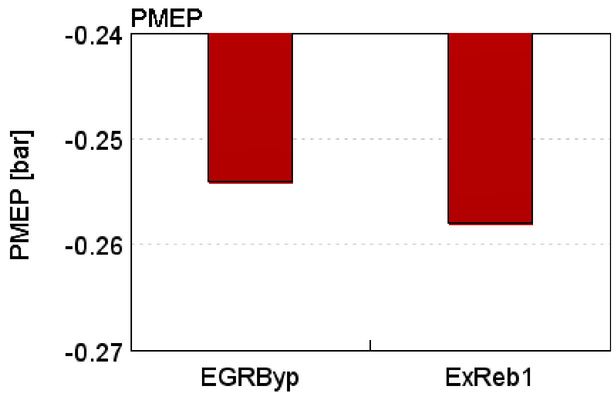

Figure 21. PMEP comparison between EGRByp and ExReb1 for Tivc 404 K at B10.

5.5. Exhaust Temperatures and Enthalpy

For low-load engine conditions, in addition to in-cylinder charge thermal promotion for enhanced combustion performance, high exhaust temperature and enthalpy are also desirable to achieve an adequate aftertreatment system performance. Hence, the potential of VVA strategies to increase exhaust temperature and enthalpy was also investigated.

Figure 22a,b compare the TrbOut T and the exhaust enthalpy [%] (defined as the percent of the total fuel energy input) trends, respectively, with respect to the BSFC among the EEVO, PVO, and ExReb1 strategies. First, all the three VVA strategies enabled a minimum TrbOut T level near 573 K, which was well above the oxidation catalyst light-off temperature threshold (523 K) in the EAT system [16].

The EEVO strategy demonstrated TrbOut T of 573 and 603 K at BSFCs of 320 and 380 g/kWh, respectively. For the similar TrbOut T levels, ExReb1 showed ~11% and 18% lower BSFC compared to the EEVO strategy. The reduced fueling penalty for ExReb1 was primarily attributed to the efficient gas-exchange process, as discussed previously. Furthermore, compared to the ExReb1 strategy, the PVO strategy incurred up to 4% higher BSFC for the same TrbOut T levels due to increased BPV throttling. The TrbOut T promotion capability of each strategy was directly related to its potential for reducing the in-cylinder trapped AFR. The minimum AFR achieved for the EEVO, PVO, and ExReb1 strategies were noted as 33.1, 31.2, and 28.8, respectively, at the Tivc level 446 K (Table 4). Consequently, the maximum TrbOut T of 599, 623, and 668 K were observed for the EEVO, PVO, and ExReb1 strategies, respectively.

In Figure 22b, the exhaust enthalpy [%], proportional to the exhaust mass flow rate and the exhaust temperature, exhibited similar trends as the TrbOut T. In spite of the highest total exhaust flow, the EEVO strategy produced a modest exhaust enthalpy increase (~1.5%) due primarily to a moderate increase in TrbOut T from relatively leaner AFR. For the PVO strategy, the exhaust enthalpies were relatively lower for int.EGR portions below 30% due to reduced total engine flow resulting from the BPV throttling. At the int.EGR portion of 39%, the PVO strategy demonstrated enthalpy level similar to ExReb1, derived primarily from the increase in TrbOut T from lower AFR. As expected, the ExReb strategy produced the largest exhaust enthalpy increase, primarily originating from the TrbOut T trends observed in Figure 22a.

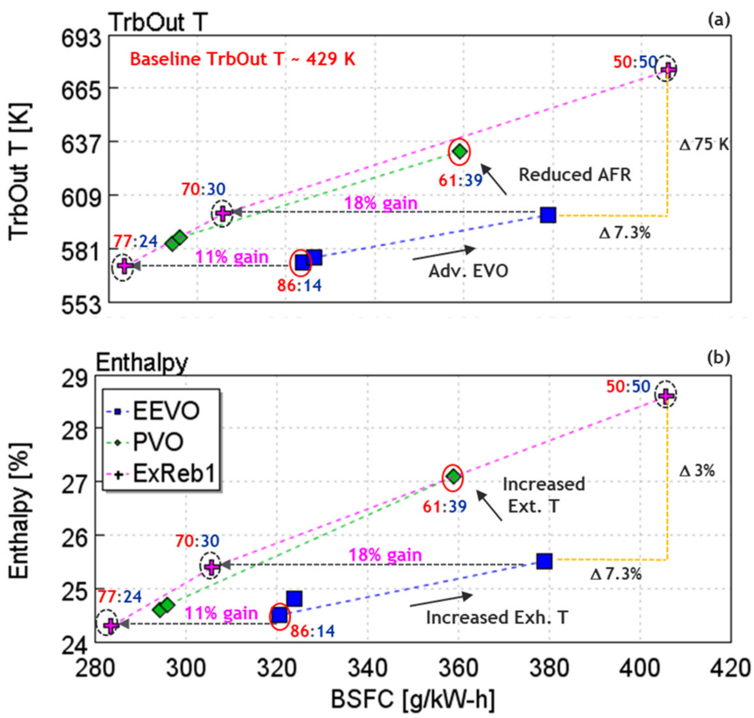

Figure 22. Comparison of all VVA strategies in terms of (**a**) TrbOut T and (**b**) exhaust enthalpy increase trends with respect to BSFC (for the elevated Tivc levels from Table 4).

6. Conclusions

The potential of VVA strategies for in-cylinder charge thermal promotion, exhaust temperature, and enthalpy increase was evaluated at the 1375 RPM and 2 bar BMEP (B10) condition in a HD GCI engine. By using close-coupled 1-D system-level analysis and 3-D CFD modeling, a numerical investigation was conducted to compare VVA strategies including EEVO, PVO, and ExReb. Key conclusions are summarized as follows:

The EEVO strategy was able to effectively increase Tsoi by 50–130 K for the BSFC range of 320–380 g/kWh. High BSFC penalties were primarily attributed to the deteriorated gas-exchange efficiency due to recompression of trapped residuals during the exhaust stroke.

The ExReb strategy demonstrated ~11% and ~18% lower BSFCs than EEVO for the similar Tsoi gains, due to a more efficient gas-exchange process. For the PVO strategy, up to 4% higher BSFCs were observed because of increased BPV throttling, compared to ExReb.

The uncooled HP EGR flow enabled Tivc of 404 K, adequate for efficient GCI combustion and a negligible increase in fueling penalty. However, the strategy could not deliver any further increase in Tivc, thus highlighting its practical limitation.

All three VVA strategies demonstrated the minimum TrbOut T near ~573 K with the highest temperature of 671 K achieved by the ExReb1 strategy. The ExReb strategy demonstrated the highest fuel efficiency among the three strategies at a given TrbOut T and enthalpy level.

The performance of exhaust rebreathe was most effective in terms of rebreathe flow versus PMEP when phased during the center of the intake stroke. In addition, extended duration was preferred over the high peak lift at a given effective valve area, to simultaneously increase rebreathe flow and reduce PMEP.

Author Contributions: P.K. and Y.Z. contributed to the conception and design of the study. Y.Z. contributed to the 3-D CFD analysis and low-NOx boundary conditions designs. P.K. implemented and established a high-fidelity 1-D and 3-D CFD close-coupling methodology. P.K. carried out the 1-D system level analysis and authored the first draft of the manuscript. All authors have read and agreed to the published version of the manuscript.

Funding: This work was funded by Aramco Americas, under the program budget for low-NOx HD GCI.

Acknowledgments: The authors gratefully acknowledge Mark Sellnau at Aramco Americas, for invaluable guidance on the subject. The authors acknowledge Sriram Popuri, from Advanced System Integration team at Cummins Technical Center for technical support and discussions. The authors also acknowledge Marko Ulaj from Aramco Americas IT support team, for his prompt support in maintaining smooth network operations during the simulation campaign.

Conflicts of Interest: The authors declare no conflict of interest. The funders had no role in the design of the study; in the collection, analyses, or interpretation of data; in the writing of the manuscript; or in the decision to publish the results.

Abbreviations

AFR	Air-Fuel Ratio
AHRR	Apparent Heat Release Rate
BR	Burn Rate
BPV	Back Pressure Valve
BSFC	Brake Specific Fuel Consumption
CAD	Crank Angle Degrees
CA50	Crank Angle at 50% Fuel Burnt
GCI	Gasoline Compression Ignition
EEVO	Early Exhaust Valve Open
EAT	Engine Aftertreatment System
ExReb	Exhaust Rebreathe
Ext.EGR	External Exhaust Gas Recirculation
EGRByp	HP EGR Cooler Bypass
EO-NO_X	Engine-Out NOx
MPRR	Maximum Pressure Rise Rate
Int.EGR, Ext.EGR	Internal, External Exhaust Gas Recirculation
IMP	Intake Manifold Pressure
IVC	Intake Valve Close
ITEg%	Gross Indicated Thermal Efficiency
PCP	Peak Cylinder Pressure
PMEP, BMEP, IMEPg	Pumping, Brake, Gross Indicated Mean Effective Pressure
PVO	Positive Valve Overlap
RSG	Residual Gas Mass Fraction
RON	Research Octane Number
ROI	Rate of Injection
SOI	Start of Injection
TDC, TDCF	Top Dead Center, Top Dead Center Firing
Tivc, Pivc	Temperature, Pressure at Intake Valve Closing
TrbOut T	Turbine-Out Temperature
Tsoi	Temperature at Start of Injection
VVA	Variable Valve Actuation

Appendix A

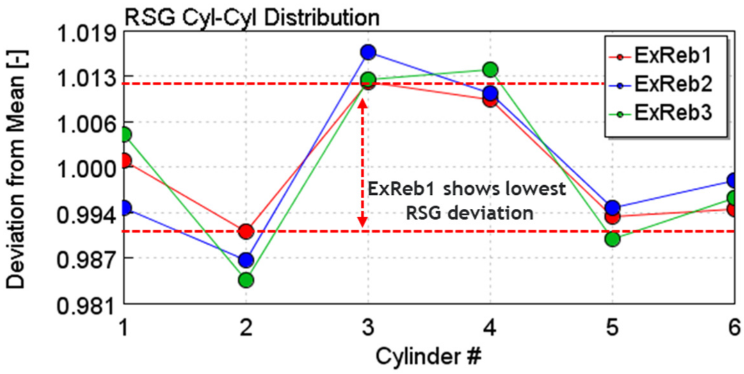

Figure A1. Comparison of total residual cylinder-to-cylinder variations among the exhaust rebreathe strategies at the total residual gas split 50:50.

Table A1. Effects on temperature and BSFC for different valve actuation strategies at B10.

TrbOut T vs. BSFC						
	EEVO		PVO		ExReb	
Tivc [K]	TrbOut T [K]	BSFC [g/kWh]	TrbOut T [K]	BSFC [g/kWh]	TrbOut T [K]	BSFC [g/kWh]
404	573.8	323.8	583.7	294.4	571.8	283.7
412	576.4	326.2	586.5	296.0	598.9	305.9
446	598.2	379.0	631.7	359.0	674.5	406.0

References

1. California Air Resources Board (CARB). Heavy-Duty Low-NOx Program. Available online: https://ww2.arb.ca.gov/our-work/programs/heavy-duty-low-nox (accessed on 4 February 2022).
2. Robertson, W. California Air Resources Board Heavy-Duty Truck and Engine Plans. In Proceedings of the SAE 2017 Commercial Vehicle Congress, Rosemont, IL, USA, 18–20 September 2017.
3. Joo, S.M.; Alger, T.; Chadwell, C.; De Ojeda, W.; Zuehl, J.; Gukelberger, R. A High Efficiency, Dilute Gasoline Engine for the Heavy-Duty Market. *SAE Int. J. Engines* **2012**, *5*, 1768–1789. [CrossRef]
4. Hoyer, K.; Sellnau, M.; Sinnamon, J.; Husted, H. Boost System Development for Gasoline Direct-Injection Compression-Ignition (GDCI). *SAE Int. J. Eng.* **2013**, *6*, 815–826. [CrossRef]
5. Sellnau, M.; Foster, M.; Moore, W.; Sinnamon, J.; Hoyer, K.; Klemm, W. *Pathway to 50% Brake Thermal Efficiency Using Gasoline Direct Injection Compression Ignition*; SAE Technical Paper; SAE: Byron Bay, Australia, 2019. [CrossRef]
6. Manente, V.; Zander, C.-G.; Johansson, B.; Tunestal, P.; Cannella, W. *An Advanced Internal Combustion Engine Concept for Low Emissions and High Efficiency from Idle to Max Load Using Gasoline Partially Premixed Combustion*; SAE Technical Paper; SAE: Byron Bay, Australia, 2010. [CrossRef]
7. Kalghatgi, G.; Risberg, P.; Ångström, H. *Advantages of Fuels with High Resistance to Auto-Ignition in Late-Injection, Low-Temperature, Compression Ignition Combustion*; SAE Technical Paper; SAE: Byron Bay, Australia, 2006. [CrossRef]
8. Kalghatgi, G.; Risberg, P.; Ångström, H. *Partially Pre-Mixed Auto-Ignition of Gasoline to Attain Low Smoke and Low NOx at High Load in a Compression Ignition Engine and Comparison with a Diesel Fuel*; SAE Technical Paper; SAE: Byron Bay, Australia, 2007. [CrossRef]
9. Kalghatgi, G.; Hildingsson, L.; Johansson, B. Low NOx and Low Smoke Operation of a Diesel Engine Using Gasoline-Like Fuels. *J. Eng. Gas. Turbines Power* **2010**, *132*, 092803. [CrossRef]
10. Zhang, Y.; Kumar, P.; Traver, M.; Cleary, D. Conventional and Low Temperature Combustion Using Naphtha Fuels in a Multi-Cylinder Heavy-Duty Diesel Engine. *SAE Int. J. Eng.* **2016**, *9*, 1021–1035. [CrossRef]
11. Zhang, Y.; Sommers, S.; Pei, Y.; Kumar, P.; Voice, A.; Traver, M.; Cleary, D. *Mixing-Controlled Combustion of Conventional and Higher Reactivity Gasolines in a Multi-Cylinder Heavy-Duty Compression Ignition Engine*; SAE Technical Paper; SAE: Byron Bay, Australia, 2017. [CrossRef]
12. Zhang, Y.; Kumar, P.; Pei, Y.; Traver, M.; Cleary, D. *An Experimental and Computational Investigation of Gasoline Compression Ignition Using Conventional and Higher Reactivity Gasolines in a Multi-Cylinder Heavy-Duty Diesel Engine*; SAE Technical Paper; SAE: Byron Bay, Australia, 2018. [CrossRef]

13. Sharp, C.; Webb, C.C.; Neely, G.; Carter, M.; Yoon, S.; Henry, C. Achieving Ultra Low NOx Emissions Levels with a 2017 Heavy-Duty on-Highway TC Diesel Engine and an Advanced Technology Emissions System—Thermal Management Strategies. *SAE Int. J. Eng.* **2017**, *10*, 1697–1712. [CrossRef]
14. Sharp, C.; Webb, C.C.; Yoon, S.; Carter, M.; Henry, C. Achieving Ultra Low NOx Emissions Levels with a 2017 Heavy-Duty on-Highway TC Diesel Engine—Comparison of Advanced Technology Approaches. *SAE Int. J. Eng.* **2017**, *10*, 1722–1735. [CrossRef]
15. Sharp, C.; Webb, C.C.; Neely, G.; Sarlashkar, J.V.; Rengarajan, S.B.; Yoon, S.; Henry, C.; Zavala, B. Achieving Ultra Low NOx Emissions Levels with a 2017 Heavy-Duty On-Highway TC Diesel Engine and an Advanced Technology Emissions System—NOx Management Strategies. *SAE Int. J. Eng.* **2017**, *10*, 1736–1748. [CrossRef]
16. Kovacs, D.; Rauch, H.; Rezaei, R.; Huang, Y.; Harris, T. *Modeling Heavy-Duty Engine Thermal Management Technologies to Meet Future Cold Start Requirements*; SAE Technical Paper; SAE: Byron Bay, Australia, 2019. [CrossRef]
17. Roberts, C.; Stanglmaier, R. *Investigation of Intake Timing Effects on the Cold Start Behavior of a Spark Ignition Engine*; SAE Technical Paper; SAE: Byron Bay, Australia, 1999. [CrossRef]
18. Leone, T.G.; Pozar, M. *Fuel Economy Benefit of Cylinder Deactivation-Sensitivity to Vehicle Application and Operating Constraints*; SAE Technical Paper; SAE: Byron Bay, Australia, 2001. [CrossRef]
19. He, X.; Durrett, P.R.; Zongxuan, S. Late Intake Valve Closing as an Emissions Control Strategy at Tier 2 bin 5 Engine-Out NOx level. *SAE Int. J. Eng.* **2009**, *1*, 427–443. [CrossRef]
20. De Ojeda, W. *Effect of Variable Valve Timing on Diesel Combustion Characteristics*; SAE Technical Paper; SAE: Byron Bay, Australia, 2010.
21. Gehrke, S.; Kovacs, D.; Eilts, P.; Rempel, A.; Eckert, P. Investigation of VVA-Based Exhaust Management Strategies by Means of a HD Single Cylinder Research Engine and Rapid Prototyping Systems. *SAE Int. J. Commer. Veh.* **2013**, *6*, 47–61. [CrossRef]
22. Hirschmann, S.; Malischewski, T.; Haubold, U.; Tilch, B. Variable Valve Trains in Heavy-Duty Engines-Benefit and Design. In Proceedings of the Heavy-Duty, On- and Off-Highway Engines Conference, Neu-Ulm, Germany, 22–23 November 2016. Available online: https://link.springer.com/book/10.1007/978-3-658-19012-5?noAccess=true (accessed on 4 February 2022).
23. Ratzberger, R.; Kraxner, T.; Pramhas, J.; Hadl, K.; Eichlseder, H.; Buergler, L. Evaluation of Valve Train Variability in Diesel Engines. *SAE Int. J. Engines* **2015**, *8*, 2379–2393. [CrossRef]
24. Ding, C.; Roberts, L.; Fain, D.J.; Ramesh, A.K.; Shaver, G.M.; McCarthy, J.; Nielsen, D. Fuel Efficient Exhaust Thermal Management for Compression Ignition Engines during Idle via Cylinder Deactivation and Flexible Valve Actuation. *Int. J. Engine Res.* **2017**, *17*, 619–630. [CrossRef]
25. Gosala, D.B.; Ramesh, A.K.; Allen, C.M.; Joshi, M.C.; Taylor, A.H.; Van Voorhis, M.; Shaver, G.M.; Farrell, L.; Koeberlein, E.; McCarthy, J., Jr.; et al. Diesel Engine Aftertreatment Warm-Up through Early Exhaust Valve Opening and Internal Exhaust Gas Recirculation during Idle Operation. *Int. J. Engine Res.* **2018**, *19*, 758–773. [CrossRef]
26. Ramesh, A.K.; E Odstrcil, T.; Gosala, D.B.; Shaver, G.M.; Nayyar, S.; Koeberlein, E.; McCarthy, J., Jr. Reverse Breathing in Diesel Engines for Aftertreatment Thermal Management. *Int. J. Engine Res.* **2019**, *20*, 862–876. [CrossRef]
27. *GT-Power Software—GT-ISE Version 2020*; Gamma Technologies Inc.: Westmont, IL, USA, 2018.
28. Kumar, P.; Zhang, Y.; Traver, M.; Watson, J. *System-Level 1-D Analysis to Investigate Variable Valve Actuation Benefits in a Heavy-Duty Gasoline Compression Ignition Engine*; SAE Technical Paper; SAE: Byron Bay, Australia, 2020. [CrossRef]
29. Kumar, P.; Pei, Y.; Traver, M.; Watson, J. *System Level 1-D Analysis of an Air-System for a Heavy-Duty Gasoline Compression Ignition Engine*; SAE Technical Paper; SAE: Byron Bay, Australia, 2019. [CrossRef]
30. CONVERGE Theory Manual v2.3. Available online: https://convergecfd.com/ (accessed on 4 February 2022).
31. Zhang, Y.; Pei, Y.; Meng, T.; Traver, M.A. Computational Investigation of Piston Bowl Geometry and Injector Spray Pattern Effects on Gasoline Compression Ignition in a Heavy-Duty Diesel Engine. In Proceedings of the ASME Internal Combustion Engine Division Fall Technical Conference, Chicago, IL, USA, 20–23 October 2019. [CrossRef]
32. Liu, Y.; Jia, M.; Xie, M.; Pang, B. Enhancement on a Skeletal Kinetic Model for Primary Reference Fuel Oxidation by Using a Semi-decoupling Methodology. *Energy Fuels* **2012**, *26*, 7069–7083. [CrossRef]
33. Kumar, P.; Sellnau, M. *EGR System Optimization for Light-Duty Gasoline Compression Ignition (GCI) Engine*; SAE Technical Paper; SAE: Byron Bay, Australia, 2021. [CrossRef]
34. Volvo Penta. Volvo Penta Reveals New 5 and 13-Liter Engines for Stage V. Press Release. 2017. Available online: https://www.volvopenta.com/industrialoffroad/en-en/news/2017/nov/volvo-penta-reveals-new-5-and-13-L-engines-for-stage-v.html (accessed on 4 February 2022).